Supplemental Methods:

Cell culture

MEFs were collected from E13.5 embryos of wild-type and Cyrano-knockout C57BL/6J mice (Kleaveland et al. 2018). Freshly harvested embryo bodies were minced in 1 mL 0.25% Trypsin-EDTA (Life Technologies) and incubated at 37°C for 30–45 min. Trypsin was then quenched by adding 4 mL MEF media (Dulbecco's Modified Eagle Medium (DMEM, VWR) with 10% Fetal Bovine Serum (FBS, Takara) and 100 U/mL penicillin/streptavidin (pen/strep, Gibco)), and cells were dissociated by pipetting up and down. Suspended cells were transferred to a 10 cm dish, 6 mL of MEF media was added, and cells were allowed to grow to confluency before initiating passaging. MEFs were then immortalized with a retrovirus expressing the HPV type 16 E6/E7 genes and the selectable marker neomycin (Halbert et al. 1991). The retrovirus was produced by PA317 LXSN 16E6E7 cells grown in DMEM with high glucose (4 mM Glutamine), and purified from the cellular supernatant by centrifugation (3000 rpm for 15 min) followed by filtration through a Millex-HV 0.45 µm syringe filter. The retrovirus titer was then measured, and the retrovirus was added to the MEFs at an MOI of 0.004 to obtain a polyclonal population with >99% single integrations. Immortalized cells were selected by continued passaging in the presence of the antibiotic G418 for three weeks. Following immortalization, MEF lines were grown at 37°C, 5% CO_2 in DMEM and 10% FBS. MEFs were passaged every 2–3 d, using 0.25% Trypsin-EDTA for dissociation.

The v6.5 mESC line was cultured at 37°C, 5% CO_2 on plates coated with 0.2% gelatin (Sigma, St. Louis, MO) in 2i media (1X DMEM/F12 (Gibco), 0.5X B27 supplement (Gibco), 0.5X N2 supplement (Gibco), 0.5X GlutaMAX (Thermo Fisher Scientific), 1X MEM NEAA (Gibco), 0.0025% BSA Fraction V (Gibco), 0.1 mM BME (Sigma), 100 U/mL U Pen/Strep, 1000 U/mL LIF (Millipore), 1µM PD0325901 (Stemgent), 3 µM CHIR99021 (Stemgent)). Cells were passaged and split 1:20 every 2 days. For passaging, cells were first washed with $–CaCl_2$, $–MgCl_2$ PBS (Thermo Fisher Scientific) and then dissociated with TrypLE Express (Thermo Fisher Scientific). Dissociated cells were resuspended in Serum/LIF media (1X DMEM KO (Gibco), 15% FBS, 1X MEM NEAA, 100 U/mL Pen/Strep, 1X GlutaMAX, 0.11 mM BME, and 1000 U/mL U LIF), pelleted by spinning at 1000g for 3 min, and resuspended in DMEM/F12 media for plating.

Cells were counted using a Countess automated cell counter (Invitrogen). To determine doubling times for the different cell lines, cells were plated and then counted at intervals following plating. These data were then fit to a single-exponential function to extract doubling time, which was determined to be

22.48 h for dividing MEFs and 9.34 h for mESCs. The doubling time for contact-inhibited MEFs was assumed to be infinite.

RNA extraction and small-RNA enrichment

Samples were thawed and then phase-separated with the addition of chloroform (J.T. Baker Analytical) at a ratio of 250 µL per 1 mL TRI Reagent. RNA was then precipitated with isopropanol, and pellets were washed twice with 70% ethanol prior to resuspension in water. Following RNA extraction, the quantitative standards were added to a level of 1 fmole/20 ng of total RNA (contact-inhibited MEFs replicate 1), 1 fmole/10 ng of total RNA (dividing MEFs replicate 1), or 1 fmole/1 ng of total RNA (contact-inhibited and dividing MEFs replicate 2, mESCs replicates 1 and 2). For the MEF samples, small RNAs were enriched from the total RNA sample with the miRvana miRNA isolation kit (Thermo Fisher Scientific). Following small-RNA enrichment, RNA was precipitated and resuspended in water.

Generating 5EU-containing quantitative standards

DNA oligos used for in vitro transcription (Supplemental Table S3) were annealed in a 100 µl reaction containing 40 µM of each oligo and 0.15 M NaCl, which was heated to 95°C for 5 min and then cooled to room temperature. Annealed duplexes were diluted to 1 µM in 0.1M NaCl and transcription was then carried out with the T7 MEGAshortscript kit (Thermofisher Scientific). To label standards with 5EU, 5EUTP (Jena Bioscience) was diluted to 75 mM in water and used in place of the UTP stock solution. After incubation at 37°C for 4 h, transcription reactions were phenol–chloroform extracted, and the desired transcript was purified on a 10% polyacrylamide urea gel and resuspended in water at a concentration of 5 µM.

Five pmol of each standard was dephosphorylated in a 100 µL reaction of 1x CutSmart Buffer (NEB) with 5 units of calf intestinal alkaline phosphatase (CIP, NEB) for 30 min at 37°C, phenol–chloroform extracted to quench the CIP reaction, ethanol precipitated to reduce the volume to 7 µL, and then labeled, according to the manufacturer's protocol, with T4 Polynucleotide Kinase (PNK, NEB) and 1µL of 25 µM γ^{32}P-ATP (Perkin Elmer) for at least 1 h at 37°C. Labeled samples were de-salted with a P30 column (Bio-Rad laboratories) and then purified on a 10% polyacrylamide urea gel.

Assessing pulldown selectivity and efficiency

Pulldown selectivity and efficiency was assessed by examining the behavior of the quantitative radiolabeled standards. Ten percent of the input, flow-through, and elution fractions from the pulldown were run out on a 15% polyacrylamide urea gel, and recovery of the standards was quantified by phosphorimaging (Typhoon FLA 7000, GE Healthcare). Enrichment of 5EU-containing standards was also assessed for each time point from the sequencing data.

Small-RNA sequencing

Samples for library preparation were assembled by mixing either 2–5 μg of total RNA (input libraries) or the entire eluate from 5EU pulldown (5EU libraries) with size-selection markers and quantitative sequencing standards. Size-selection markers were 18 and 32 nt 5'-end-labeled RNAs (Supplemental Table S3). Sequencing standards (Supplemental Table S3) were added at a level of either 0.1 fmol per 1 μg total RNA (input libraries) or 2.5 amol per sample (5EU libraries). Both 3' and 5' ligations were carried out with degenerate adaptors (each containing four random nucleotides at the ligation junction) in the presence of 10% Polyethylene Glycol (PEG 8000, NEB) and 0.5 μL of Superasin (Thermo Fisher Scientific) with either T4 RNA-ligase 2, truncated K227Q (NEB) or T4 RNA-ligase 1 (NEB), respectively. Reverse transcription was with SuperScript III (NEB), and subsequent PCR amplification of the cDNA was with Phusion (NEB). A step-by-step protocol for preparing small-RNA sequencing libraries is available at http://bartellab.wi.mit.edu/protocols.html. Samples were sequenced on an Illumina HiSeq platform with 40-nt single-end reads.

Sequencing reads were trimmed at the 5' and 3' ends using fastx_trimmer (FastX Toolkit; http://hannonlab.cshl.edu/fastx_toolkit/) and cutadapt (Martin 2011), respectively. Trimmed reads were subsequently filtered for greater than 99.9% accuracy for all bases using fastq_quality_filter (FastX Toolkit) with the parameters '-q 30 –p 100'. To call miRNA reads, the first 19 nucleotides of filtered and trimmed reads were string-matched to a dictionary of miRNA sequences. The miRNA dictionary was curated by filtering miRbase_v21 miRNA annotations for all conserved or confidently annotated small RNA species (as annotated by TargetScanMouse, release 7.2; http://www.targetscan.org/mmu_72/) as well as their passenger-strand partners (Supplemental Tables S1,2). Although most miRNAs have a unique initial 19 nucleotides, a few species cannot be called unambiguously using only the first 19 nucleotides. These species were collapsed into a single dictionary entry (whose sequence was chosen randomly to be one of the collapsed species' sequence) and listed under a merged name (for example, mmu-miR-199a-3p and mmu-miR-199b-3p become mmu-miR-

199ab-3p). Assigned reads were normalized within each time course using either the 5EU-containing quantitative standards (5EU data) or the sequencing standards (input data). Each miRNA in the normalized 5EU dataset was then further normalized to its abundances across the normalized input dataset to account for any potential non-steady-state behavior. With the exception of the passenger and guide comparisons, all analyses were carried out with only the guide strands; for each miRNA duplex, guide strands were distinguished from passenger strands based on abundance in the input libraries.

For trimming and tailing analyses, suffixes to the 19 nucleotide prefixes were enumerated for each miRNA. All suffixes representing more than 20% of the reads for a miRNA in the 1 h 5EU time interval were designated initial products of biogenesis (Supplemental Table S1), and the trimmed and tailed suffixes were annotated with respect to their respective initial isoform. Only guide RNAs with one initial isoform were used when modeling isoform dynamics.

RNA sequencing

RNA-seq samples were prepared using the NEXTflex Rapid Directional mRNA-seq Kit (Bioo Scientific). Briefly, mRNAs were enriched from 10 µg total RNA with NEXTflex Poly(A) Beads (Bioo Scientific). These species were then fragmented, synthesized into cDNA, ligated to adaptors, and PCR amplified as per the manufacturer's protocol. Samples were then sequenced on an Illumina HiSeq platform with 40-nt single-end reads.

Reads from MEFs and mESCs were aligned to the mouse genome (mm10) with Star v. 2.4 with the parameters "--alignIntronMax 1 --runThreadN 30 --outFilterMultimapNmax 1 --outFilterMismatchNoverLmax 0.04 --outFilterIntronMotifs RemoveNoncanonicalUnannotated --outSJfilterReads Unique". These reads were then assigned to genes based on annotations from Ensembl (Mus_musculus.GRCm38.94.gtf downloaded September 5, 2018) with htseq-count v0.9.1 (Anders et al. 2015) with the parameters '-m union –s reverse'. Targets present in the different cell lines were identified and classified based on TargetScanMouse v7.2 annotations. Raw RNA-seq reads from mouse 3T9 fibroblasts (Ghini et al. 2018) were downloaded from the GEO (GSE104650) and processed as described above, except the parameters '-m union –s no' were used for htseq-count, which accommodated the non-stranded 3T9 dataset.

Northern blotting

After resolving 5–10 μg of total RNA on a 20% polyacrylamide urea gel, RNA was transferred to a Hybond-NX membrane (GE Healthcare) with a semi-dry transfer apparatus (Bio-Rad) and crosslinked to the membrane by incubation with EDC (*N*-(3-dimethylaminopropyl)-*N*′-ethylcarbodiimide; Thermo Scientific) diluted in 1-methylimidazole for 1–2 h at 60˚C. Blots were probed with either DNA or LNA oligonucleotide probes (Supplemental Table S3). Results were quantified using ImageQuant TL (v8.1.0.0). A step-by-step protocol can be found at http://bartellab.wi.mit.edu/protocols.html.

Pulse-labeling with heavy amino acids and AGO isolation

SILAC media were prepared essentially as described (Ong and Mann 2006). DMEF base media was made by mixing DMEM lacking Lysine and Arginine (Thermo Fischer Scientific) with dialyzed FBS (Life Technologies). Base media for mESCs was made with DMEM/F-12 lacking Lysine and Arginine (Life Technologies) plus all additional components required for mESC culture as listed above. These base media were then supplemented with 84 mg/mL $^{13}C_6{}^{15}N_4$ L-arginine plus 146 mg/mL $^{13}C_6{}^{15}N_2$ L-lysine or the corresponding non-labeled amino acids (all from Sigma) to generate either heavy or light media, respectively. MEFs and mESCs were grown in light SILAC medium for at least five passages prior to pulse-labeling. Contact-inhibited MEFs were seeded onto 10 cm dishes and allowed to reach a contact-inhibited state 5 days prior to the start of the pulse labeling, whereas dividing MEFs and mESCs were plated at a density of 225,000 cells per 10 cm dish or 200,000 cells per 15 cm dish, respectively, 48 h prior to the planned time of collection. At time zero, the light media was removed, and cells were washed three times with pre-warmed PBS before transfer into heavy media. Cells were collected 1.5, 4.5, 14, and 24 h after growth in heavy media and washed twice with ice-cold PBS, scraped off the plate, spun down, and snap frozen.

Frozen pellets were resuspended in 500 µL of NET buffer (50 mM Tris, pH 7.5, 150 mM NaCl, 5 mM EDTA, 0.5% NP-40, 10% glycerol, 1 mM Sodium Orthovanadate, 0.5 mM DTT; supplemented with cOmplete EDTA-free Protease Inhibitor Cocktail (Roche)) and incubated at 4°C for 20 min. The lysate was then passed through a 23G syringe seven times before centrifugation at 15,000g for 20 min. AGO proteins were enriched based on their affinity to a peptide derived from TNRC6 (T6B) as described (Hauptmann et al. 2015). Briefly, Protein G beads (Life Technologies) were washed once with PBST (PBS, 0.02% Tween) before being incubated with anti-FLAG antibody (Sigma Aldrich) at room temperature with end-over-end rotation for 10 min. The beads were then washed twice with PBST before incubation

with FLAG-tagged T6B peptide at 4°C with rotation for 2 h. Peptide-coupled beads were washed three times with PBS, and then resuspended in cell lysate and rotated at 4°C for 3 h. Beads were then washed four times with NET buffer, once with PBS, and then resuspended in NuPAGE 2x LDS Sample buffer (ThermoFischer Scientific).

Mass spectrometry and AGO2 half-life estimation

AGO-enriched samples were incubated at 95°C for 5 min and then resolved on a 4-12% Bis-Tris NuPAGE gel (Thermo Fischer Scientific). Gels were stained with Imperial Protein Stain (Thermo Fischer Scientific), and a band migrating near 100 kDa was excised, cut into ~2mm squares, and washed overnight in 50% methanol. The following day the gel pieces were washed once more with a solution of 47.5% methanol, 5% acetic acid for 2 h before being dehydrated with acetonitrile and dried in a speed-vac. Gel pieces were then incubated in 30 µL 100 mM ammonium bicarbonate with 10 mM dithiothreitol for 30 min to reduce disulfide bonds, before subsequent incubation in 30 µL of 100 mM ammonium bicarbonate and 100 mM iodoacetmide for cysteine alkylation. Gel pieces were then sequentially washed with acetonitrile, 100 mM ammonium bicarbonate and acetonitrile and dried in a speed-vac. Gel pieces were subsequently rehydrated with a sufficient volume of 50 mM ammonium bicarbonate, and trypsin was then added to a final concentration of 20 ng/µL trypsin. Following addition of the trypsin, samples were first incubated on ice for 10 minutes before digestion overnight at 37°C with gentle shaking. The digested peptides were extracted by serial 10 min incubations at 37°C with shaking in 50 µL 50 mM ammonium bicarbonate, 50 µL of a solution of 47.5% acetonitrile, 5% water, and 5% formic acid, and 50 µL of acetonitrile/formic acid solution once again. The supernatants from each incubation were pooled, organic solvent was removed, and sample volumes were reduced to 15 µL using a speed vac.

Samples were next analyzed by reversed-phase high-performance liquid chromatography (HPLC) using a Thermo EASY-nLC 1200 HPLC equipped with a self-packed Aeris 1.7 µm C18 analytical column (0.075 mm by 14 cm, Phenomenex). Peptides were eluted using standard reverse-phase gradients, and effluent was analyzed using a Thermo Q Exactive HF-X Hybrid Quadrupole-Orbitrap mass spectrometer (nanospray configuration) operated in a data-dependent manner. The resulting fragmentation spectra were correlated against the known database using PEAKS Studio X (Bioinformatic Solutions).

Heavy-to-light ratios were computed for all AGO2 peptides that had peak areas greater than 10,000 for both heavy and light peptides at all time points. These ratios were used to determine the disappearance

rate constant of AGO2 by fitting the data to the following model: $ln(r+1) = k_d(t - t_0)$, where r is the ratio of the peak areas for heavy and light isotopes of each individual peptide, k_d is the disappearance rate constant, t is the time, and t_0 is the time offset due to the lag in heavy-isotope incorporation following the media change (Schwanhäusser et al. 2011). The parameters k_d and x_0 were fit by using the optim function in R (method="L-BFGS-B", R version 3.2.5) to minimize the sum of the squared residuals of this model to the data. All fit parameters were bounded to be > 10^{-8}. As k_d is the sum of the rate of dilution due to cell division and the rate of protein degradation, the AGO2 degradation rate constant (k_{deg}) was determined by subtracting the rate of dilution due to cell division ($ln(2)/t_{cc}$, where t_{cc} is the duration of a cell cycle) from the fit value for k_d. Values of t_{cc} for each cell-type were determined empirically. AGO2 half-life was then calculated from k_{deg} as $t_{1/2} = log(2)/k_{deg}$.

Fitting models to data

When fitting the data to extract production rates and half-lives, the optim function in R (method="L-BFGS-B", R version 3.2.5) was used to minimize the sum of the squared residuals of the log-transformed model to the log-transformed data. For each dataset, fitting was carried out globally, minimizing the sum of the residuals for all miRNAs with reads passing the expression threshold, which enabled extraction of a single value for the time-offset parameter (t_0) for the entire dataset. For the single-exponential model, the values for the rate constants of production (α) and degradation (β) for each guide RNA were fit in addition to the global t_0 value. The fit values for the rate constants were bounded to be > 10^{-8} reads h^{-1}, and the fit value for t_0 was required to be between 0.01 and 1 h. For the biexponential model, the values for one rate constant of production (α), four rate constants of degradation (β_n), and one fractional split (f) were extracted for each guide–passenger pair, in addition to the global t_0 value. When simultaneously optimizing fits to guide- and passenger-strand data, the U-bias effects were accounted for by scaling the production rates for each passenger and guide strand by the U-bias scaling factor. As a result of this scaling, the fit production rates reported for guide and passenger strands from the same duplex were usually not identical. The bounds for the production and degradation rate constants as well as for t_0 were the same as for the single-exponential models, and the value for the fractional split was bounded to be between 10^{-8} and 1. For all models, the rate of cell division (g) was manually set based on experimental determination. To ensure that the true minima was reached by the optim function, we ran the optimization for each dataset iteratively 100 times using the parameter values reached by the previous round of optimization as the starting values for the next round. When fitting the exponential model of 5EU bioavailability to the data (Supplemental Fig. S1F,G),

γ was fit globally and was constrained to be between 0.4 and 25. Otherwise, fitting was carried out as for the single-exponential model.

For the isoform analyses, fitting was again carried out by using the optim function in R (method="L-BFGS-B", bounds set to 0.000001 and 1000000 for all parameters) to minimize the sum of the squared residuals. All isoforms for a given miRNA were fit simultaneously with a system of differential equations that was solved by numerical integration with the lsoda function. Fitting was carried out in log-space, and optim was iteratively run 10 times to ensure true minimization.

Bootstrap analyses

Reads for each time course were resampled 20 times in accordance with the original read distribution across all miRNAs and the quantitative standards. These resampled datasets were then normalized and combined, in the same manner as for the original data, to generate 20 resampled time courses for each of the three original time courses (contact-inhibited MEFs, dividing MEFs and mESCs). These time courses were fit to single-exponential functions to extract production rates and half-lives. The coefficient of variation was determined for the parameter of interest for each miRNA by dividing the standard deviation of this parameter across both the original and all resampled datasets by the mean of the parameter.

Family analyses

All guide strands were assigned to families based on seed region sequence. Comparisons were then made between all pairs of family members within each family. Guide strands with capped half-lives (either > 72 h in dividing MEFs, or > 24 h in mESCs) were not considered in these analyses due to uncertainty of their true half-life values. The metrics of percent difference and Hamming distance were used to measure half-life variation and sequence similarity, respectively. Random comparisons used equal numbers of non-family pairs, selected randomly, without replacement.

Motif and feature searches

To search for motifs associated with rapid turnover, we either ranked miRNAs according to half-life or classified them into fast- and slow-turnover subsets. To search for position-specific motifs, we supplied a list of miRNA sequences ranked by half-life to kpLogo (Wu and Bartel 2017). To query differences in more general nucleotide content, we classified miRNAs as fast or slow turnover. The fast- and slow-

turnover subsets were delineated as species that had the upper or lower bounds of their 95% confidence intervals below or above certain thresholds (specified in the figure legend where applicable). Such classification ensured that the subsets compared were truly differentially turned over. Different features of these fast- and slow-turnover subsets were also compared to the analogous features for equal-size subsets of all of the miRNAs examined in this study.

Quantification and statistical analyses

Graphs were generated and statistical tests were performed using R (v3.2.5). Statistical parameters including the test used, significance ascertained (*p* value), and number of points compared (*n*) are reported in either the figures or their legends. For 5EU time courses, replicates refer to biological replicates carried out on different days. Standard deviations and confidence intervals on the fit parameters were determined by computing the covariance matrix for these parameters from the variance of the residuals and an approximation of the Hessian of the error function. Statistical tests were selected based on the comparison being made. No statistical tests were performed to pre-determine sample size. A two-sided Z-test was applied to identify miRNAs that exhibited significantly higher rates of production than expected for their abundance (significance required $|Z\text{-score}| > 2$). Based on the nature of the data, either an unpaired two-sample, two-tailed *t* test or a Mann–Whitney U test was used for comparisons of the distributions of guide and passenger half-lives, half-life percent differences, and isoform rate constants. Significance of correlations between half-life percent difference and sequence similarity for family members was assessed using a correlation test (cor.test function, method = 'pearson', R v3.2.5).

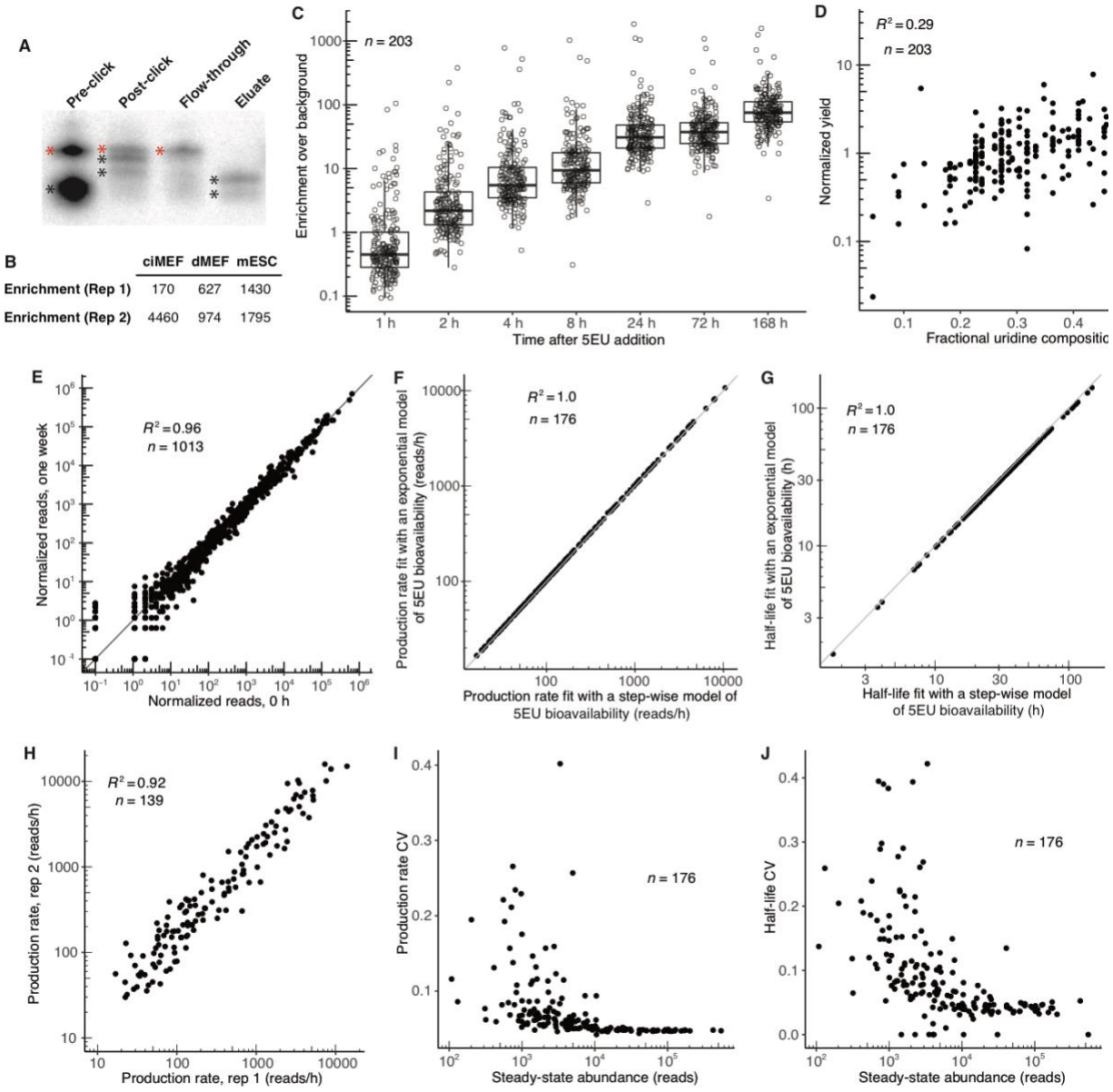

Supplemental Figure S1. Labeling with 5EU enables efficient and selective pulldown of small RNAs with minimal background or bias. (A) Selective enrichment of 5EU-containing standards. Shown is a phosphorimager scan of a denaturing acrylamide gel that resolved the three radiolabeled 22–25-nt small RNAs that each contained a single 5EU (black asterisks) and an unlabeled 30-nt RNA (red asterisks). The pre-click lane shows the ratio of these species prior to biotinylation, and the post-click lane shows that the addition of the biotin group slowed mobility of the 5EU-containing standards. The other lanes show that the flow-through was depleted in 5EU-containing standards, whereas the eluate was strongly enriched in 5EU-containing standards, which had regained their faster mobilities because the biotin group was cleaved from the RNA during elution. (B) Selective enrichment of 5EU-containing standards, as indicated by sequencing. Reported are median fold-enrichment values of 5EU-containing standards over a standard that lacked 5EU, as determined by small-RNA sequencing of samples from contact-inhibited MEFs (ciMEFs), dividing MEFs (dMEFs), and mESCs. (C) Enrichment of each individual miRNA (including each passenger strand passing the expression threshold) over its background level across time

in contact-inhibited MEFs. Background levels were determined by sequencing the RNA eluted after performing the pulldown procedure on RNA from cells that had not been metabolically labeled. (D) Relationship between pulldown yield and the number of U nucleotides in the miRNA. For each miRNA (including passenger strands) in the contact-inhibited MEF dataset, median-centered normalized yield is plotted as a function of fractional uridine composition. Pulldown yields were normalized by dividing the reads from the 1-week 5EU eluate sample by the reads from the 1-week input sample and then median centered; this normalized yield indicates the extent to which each miRNA was enriched or depleted in the 5EU dataset compared to expectation. (E) A comparison of miRNA reads in the one-week input sample to those in the unlabeled input sample (reads for all confidently annotated guide and passenger strands are shown). Reads for each sample, which were both from contact-inhibited MEFs, were normalized to the internal standards. (F–G) Correspondence of production rates (F) or half-lives (G) of guide strands fit assuming either a step-wise model of 5EU bioavailability (x-axis), or an increasing exponential model of 5EU bioavailability (y-axis). The step-wise model of 5EU bioavailability is described by the single-exponential fit with a time offset (Fig. 1B, equation (1)). The increasing exponential model is described by the following function: $y = \left(\frac{\alpha}{\beta-\gamma} - \frac{\alpha}{\beta}\right)e^{-\beta t} + \left(\frac{\alpha}{\gamma-\beta}\right)e^{-\gamma t} + \frac{\alpha}{\beta}$, where α describes the production rate, β describes the degradation rate, and γ describes the rate at which 5EU approaches its steady-state value. As with the time offset of the step-wise model, γ of the increasing exponential model was fit globally. (H) Correspondence of production rates of guide strands from the two contact-inhibited MEF replicates. (I–J) Coefficient of variation (CV) for production rates (I) or half-lives (J) determined from bootstrap analyses of the contact-inhibited MEFs data. Data were resampled 20 times, and each resampled dataset was fit to extract rates of production and degradation. These parameters were then compared with each other and with the parameters fit to the original data to derive CV values, which are plotted as a function of miRNA steady-state abundance (as measured in the 1-week input sample). As expected, CV values decreased with increasing miRNA steady-state abundance.

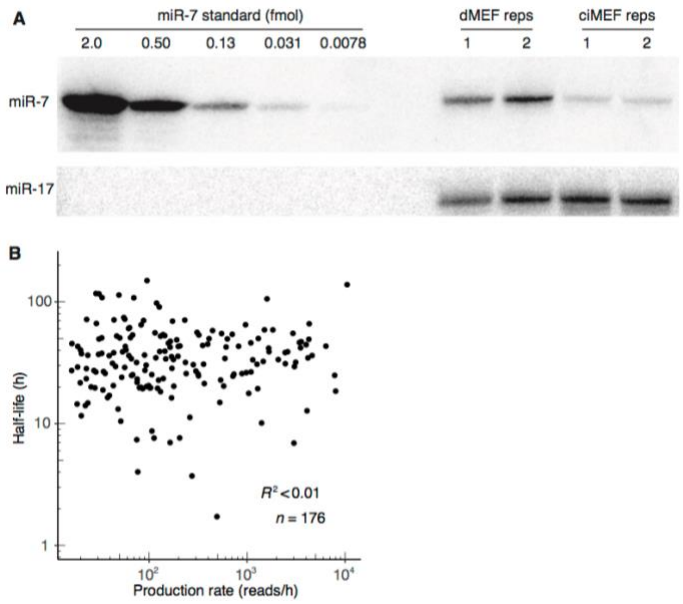

Supplemental Figure S2. Dynamics of guide miRNAs in contact-inhibited MEFs. (A) Quantitative northern blot used to determine the absolute number of miR-7 molecules in contact-inhibited and dividing MEFs (ciMEF and dMEF, respectively). 10 μg of total RNA, which corresponded to ~5 million cells, was loaded for each replicate (reps) for the dividing MEFs, and 20 μg of total RNA, which corresponded to ~10 million cells, was loaded for each replicate for the contact-inhibited MEFs. Standards of the specified molar amounts were loaded for miR-7; miR-17 served as a loading control. (B) Relationship between half-life and production rate for guide strands in contact-inhibited MEFs.

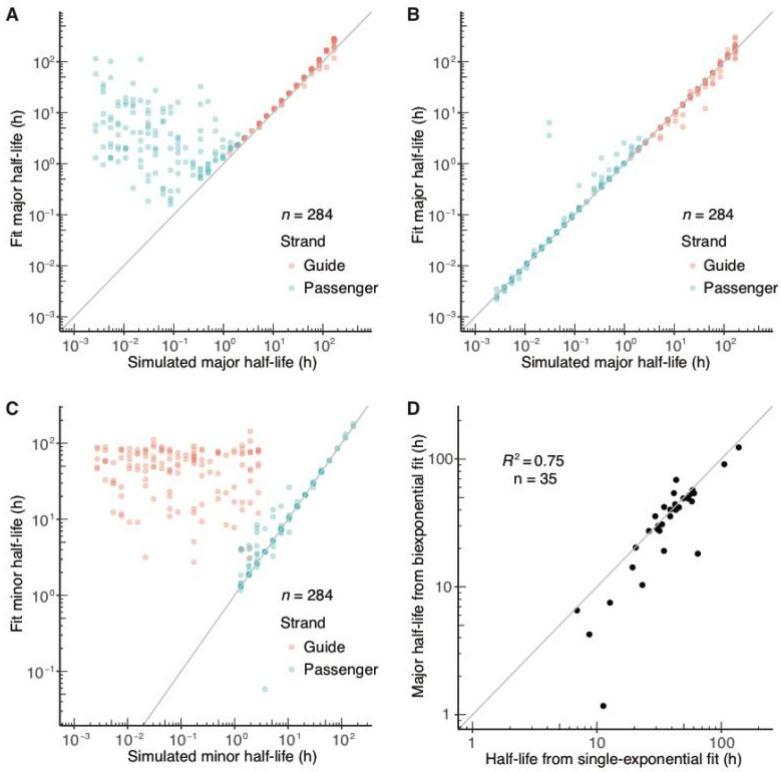

Supplemental Figure S3. Fitting passenger and guide pairs to a biexponential model. (A–C) Assessing the ability of the single-exponential fits (A) and biexponential fits (B–C) to recapitulate simulated data for both guide and passenger strands. Bi-phasic behavior was simulated with a system in which each species was divided between two behavioral populations with a specified fractional distribution (Fig. 1B, eqn. 2). Both populations of each species were set to have the same production rate, but each had an individual rate of degradation (with the "major" and "minor" rates describing the turnover of the majority or the minority of the species, respectively) (Fig. 1B, eqn. 2). A wide array of different input parameters was fed into this model to generate many different bi-phasic behaviors. Initial simulations revealed the range of half-lives that the models could accurately fit, and these bounds were applied in the simulations shown here. Major half-lives from either single-exponential fits (A) or biexponential fits (B) were compared to the major half-lives used to generate the simulated data. Additionally, minor half-lives fit using the biexponential model were compared to the minor half-lives used to generate the simulated data (C). These simulations illustrated the utility of fitting to the biexponential model when determining the half-lives of the both the major and the minor passenger-strand populations. They also showed that fitting to either model was sufficient to determine half-life of the major guide-strand population (provided that the half-life did not exceed the longest time interval) and that fitting to neither model was reliable for determining the half-life of the minor guide-strand population. (D) Correspondence between half-lives determined by biexponential fits and half-lives determined by single-exponential fits for the 35 guide strands that were members of guide–passenger pairs analyzed in contact-inhibited MEFs.

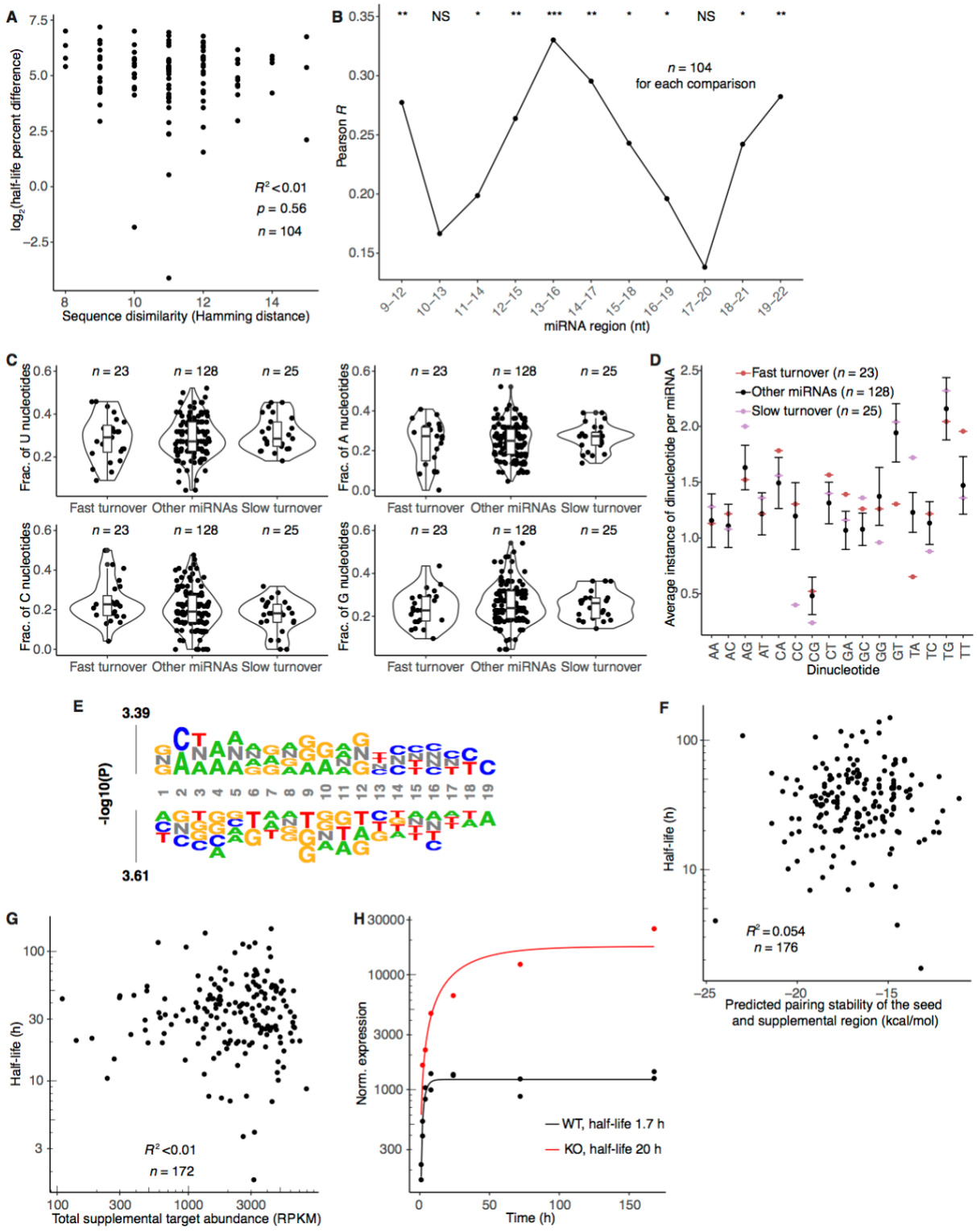

Supplemental Figure S4. Search for determinants of turnover for guide strands in contact-inhibited MEFs. (A) Relationship between half-life difference and sequence dissimilarity (as measured by Hamming distance) for random pairs of non-family members. Only nucleotides downstream of the seed region were considered for the Hamming-distance measurement; higher Hamming-distance values

indicate more dissimilar sequences. Significance of the correlation was determined by a *t* test. Twenty-five equally sized cohorts of randomly paired guides were analyzed in the same way, with the plot shown here being for the cohort with the median R^2 value. (B) Relationship between half-life percent difference and Hamming distance for 4-nt segments of family-member pairs. Plotted for each 4-nt segment downstream of the seed region is the Pearson *R* describing the correlation between these two metrics. Significance of each correlation was determined by a *t* test. (C) Nucleotide composition for fast- and slow-turnover species as well as all other miRNAs. Fast-turnover species had half-life 95% confidence intervals that fell below 35 h; slow-turnover species had half-life 95% confidence intervals that fell above 25 h; other miRNAs fit into neither of these categories. (D) Average dinucleotide composition of fast-turnover miRNAs (red), slow-turnover miRNAs (purple), and other miRNAs (black). MicroRNAs were assigned to the categories as in (C). To allow comparison between equal-sized groups of miRNAs, the 'other' miRNAs were subset into random sets that were of equal size to the fast-turnover set. The dinucleotide composition was determined for 50 of these random cohorts, and the mean composition for all cohorts is shown (error bars, standard deviation). (E) *k*-mer logo (Wu and Bartel 2017) depicting the *k*-mer at every miRNA position that is most significantly enriched (above the line) or depleted (below the line) in rapidly turned-over miRNAs. The stacked height of each *k*-mer corresponds to the $\log_{10}$-transformed *P* value for that *k*-mer; positions with *k*-mers that were significantly enriched after multiple-hypothesis testing would have appeared in red. (F) Correspondence between predicted pairing stability of the seed plus supplemental region, and miRNA half-life. (G) The relationship between half-life and summed RPKM (Reads per kilobase of transcript per million mapped reads) of all predicted targets with supplemental pairing to the miRNA. Predicted targets capable of supplemental pairing were identified as those with TargetScan7 supplementary-pairing scores < –0.05 (Agarwal et al. 2015). (H) 5EU time courses for miR-7 in wild-type (WT, black) and Cyrano-knockout (KO, red) contact-inhibited MEFs. Single-exponential fits are displayed for each time course, with the calculated half-lives noted in the key.

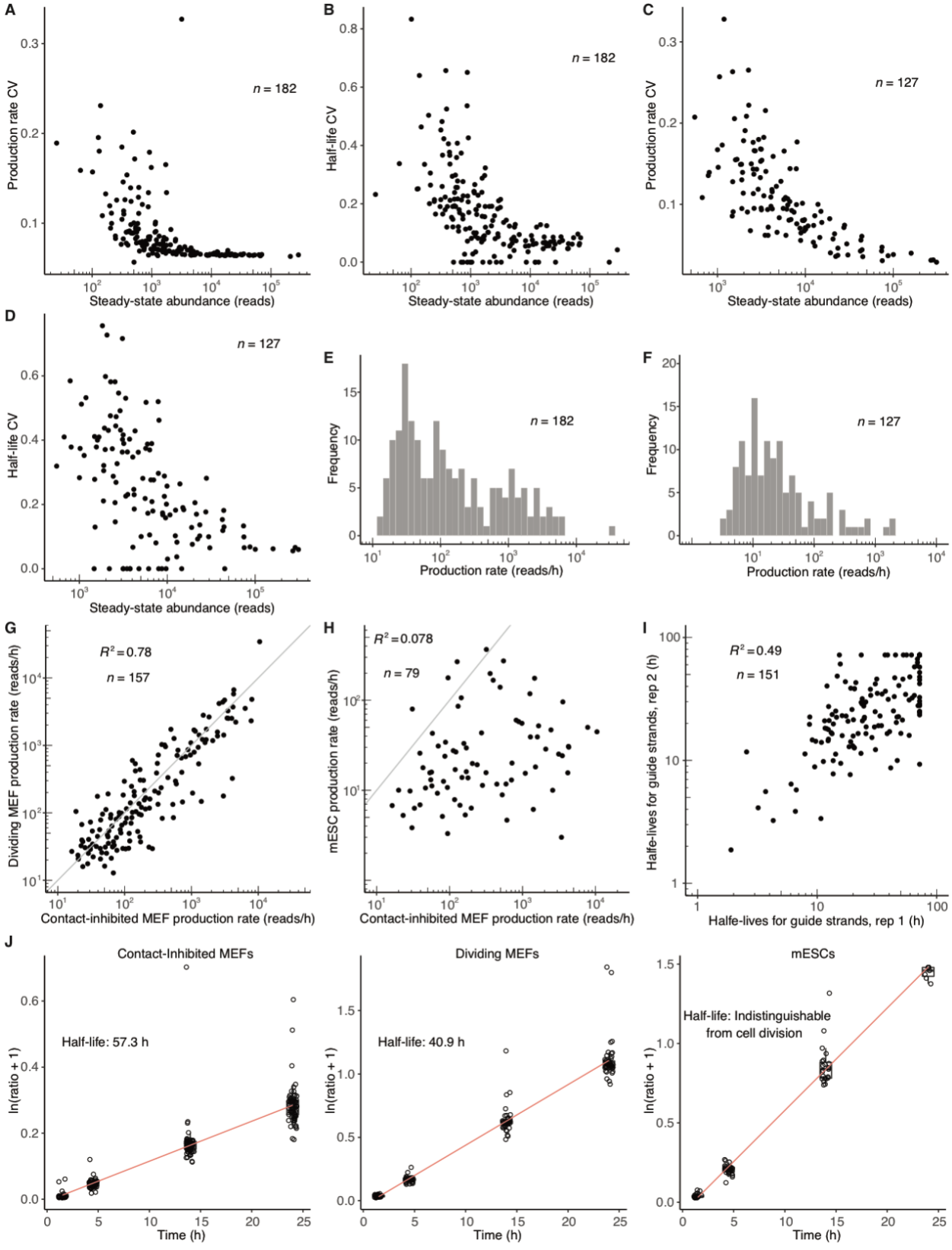
A
Production rate CV
n = 182
Steady-state abundance (reads)
B
Half-life CV
n = 182
Steady-state abundance (reads)
C
Production rate CV
n = 127
Steady-state abundance (reads)
D
Half-life CV
n = 127
Steady-state abundance (reads)
E
Frequency
n = 182
Production rate (reads/h)
F
Frequency
n = 127
Production rate (reads/h)
G
R² = 0.78
n = 157
Dividing MEF production rate (reads/h)
Contact-inhibited MEF production rate (reads/h)
H
R² = 0.078
n = 79
mESC production rate (reads/h)
Contact-inhibited MEF production rate (reads/h)
I
R² = 0.49
n = 151
Halfe-lives for guide strands, rep 2 (h)
Halfe-lives for guide strands, rep 1 (h)
J
Contact-Inhibited MEFs
Half-life: 57.3 h
Dividing MEFs
Half-life: 40.9 h
mESCs
Half-life: Indistinguishable from cell division
ln(ratio + 1)
Time (h)

Supplemental Figure S5. Dynamics of miRNA guide strands in dividing MEFs and mESCs. (A–D) Coefficients of variation determined from bootstrap analyses for production rates (A) and half-lives (B) in dividing MEFs as well as for production rates (C) and half-lives (D) in mESCs. Otherwise, as in Supplemental Fig. S1I,J. (E–F) Distribution of production rates for guide strands in dividing MEFs (E) and mESCs (F). (G–H) Relationship between guide-strand production rates in either dividing MEFs (G) or mESCs (H) and guide-strand production rates in contact inhibited MEFs. (I) Comparison of guide-strand half-lives for replicates in dividing MEFs. (J) AGO2 half-lives in contact-inhibited MEFs, dividing MEFs, and mESCs. Shown are plots of the natural-log-transformed ratios of the heavy-to-light isotopes for all AGO2 peptides identified by mass spectrometry following SILAC pulse-labeling with heavy media in each cell type. These data were fit to a linear function (red) to extract AGO2 half-lives.

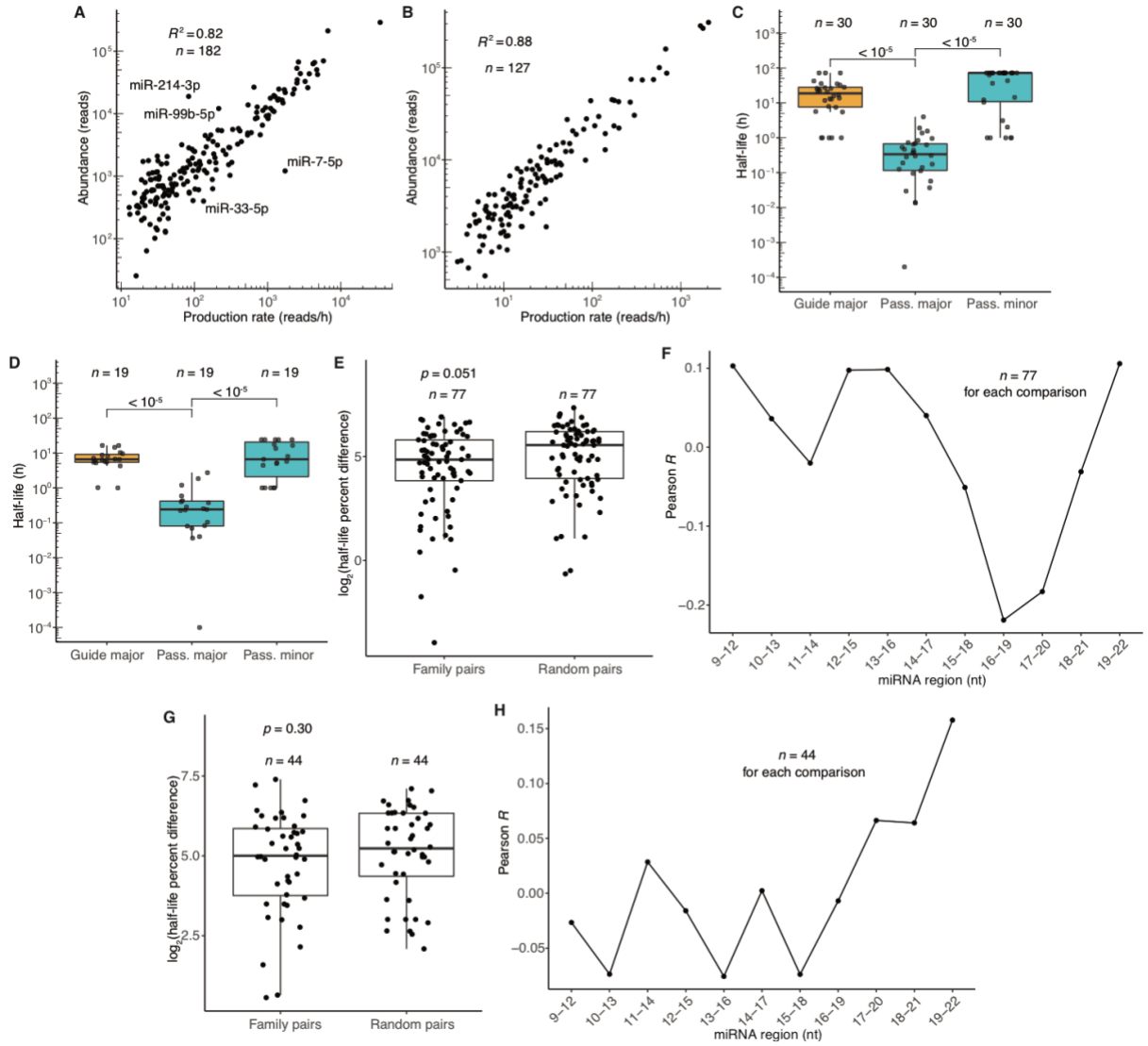

Supplemental Figure S6. Passenger-strand dynamics and determinants of half-life in dividing MEFs and mESCs. (A–B) Relationship between guide-strand production rate and steady-state miRNA abundance in dividing MEFs (A) and mESCs (B). Steady-state abundance is measured as reads in the 72 h and 24 h input sample, respectively. (C–D) Half-life distributions for guide and passenger (pass.) strands of dividing MEFs (C) and mESCs (D), determined by fitting the biexponential model. Otherwise, as in Fig. 3B. (E) Differences in half-lives for pairs of family members or randomly paired guides in dividing MEFs. Otherwise, as in Fig. 4A. (F) Relationship between half-life difference and Hamming distance for 4-nt segments of family-member pairs in dividing MEFs. Otherwise, as in Supplemental Fig. S4B. (G) As in (E) but analyzing data from mESCs. (H) As (F) but analyzing data from mESCs.

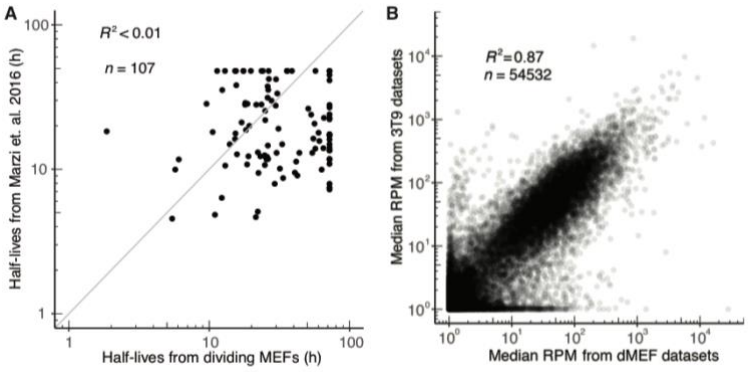

Supplemental Figure S7. Comparison of published results from dividing 3T9 mouse fibroblasts with our results from dividing MEFs. (A) Correspondence between guide-strand half-lives published for 3T9 cells (Marzi, 2016) and those obtained for dividing MEFs. (B) Correspondence between mRNA levels in dividing 3T9 cells (Ghini, 2018; GEO accession number GSE104650) and mRNA levels in dividing MEFs. Plotted are median RPM values from three and two RNA-seq replicates from 3T9 cells and dividing MEFs, respectively.

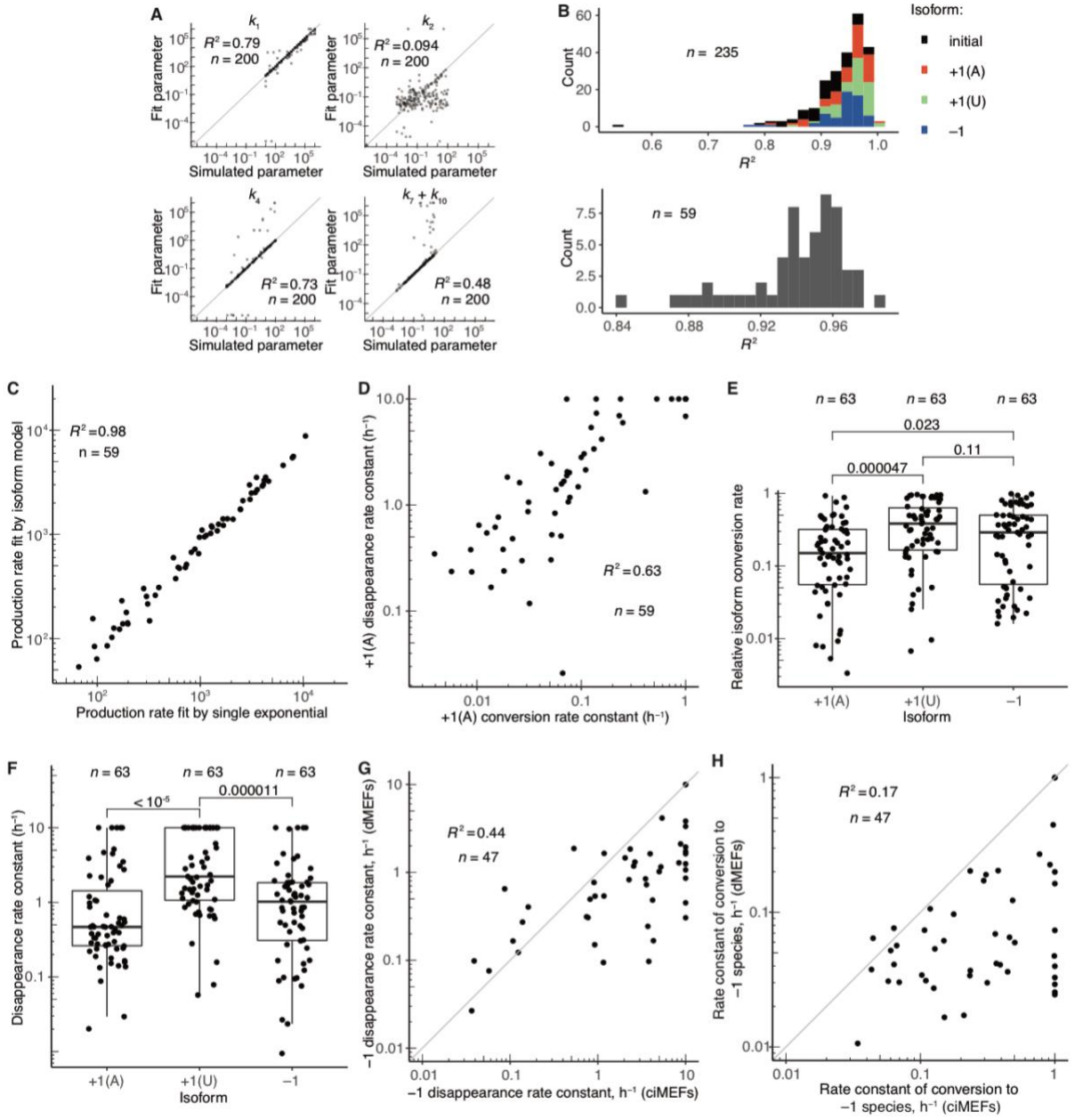

Supplemental Figure S8. Isoform dynamics in contact-inhibited and dividing MEFs. (A) Correspondence between parameter values fit to simulated data and those initially used to generate the simulated data. A wide array of parameter values was applied to the model described in Fig. 6B to generate the simulated data. Plotted are values fit to these data as a function of the initial simulated values for the rate constant of initial isoform production (k_1), the rate constant of initial isoform degradation (k_2), the rate constant for conversion of the initial isoform to the +1(U) isoform (k_4), as well as the rate constant for disappearance of the +1(U) isoform ($k_7 + k_{10}$). Although not shown, the correlations for rate constants for the conversion and disappearance of the other isoforms were similar to those observed for +1(U). (B) Stacked histograms of the R^2 values for fits to each individual isoform (top) as well as all isoforms together (bottom). (C) Relationship between miRNA production rates in contact-inhibited MEFs, comparing the production rate of the initial isoform fit to the isoform model (Fig. 6B) and the production rate of the guide RNA using the single-exponential fit (Fig. 1B). (D) Relationship between the rate

constant of disappearance of the +1(A) isoform and the rate constant of conversion to the +1(A) isoform. Because simulations indicated that conversion rate constants > 1 h^{-1} and disappearance rate constants > 10 h^{-1} could not be accurately fit, conversion and disappearance rate constants were capped at these values, respectively. (E) Relative rates of conversion to the +1(A), +1(U), or –1 isoforms in dividing MEFs. Otherwise, as in Fig. 6E. (F) Rate constants of disappearance ($k_6 + k_9$, $k_7 + k_{10}$, or $k_8 + k_{11}$) for the +1(A), +1(U), or –1 isoform, respectively, in dividing MEFs. Otherwise, as in Fig. 6F. (G) Correspondence between rate constants of disappearance of –1 ($k_8 + k_{11}$) in dividing MEFs (dMEFs) and contact-inhibited MEFs (ciMEFs). (H) Correspondence between rate constants of conversion to the –1 isoform (k_5) in dividing MEFs (dMEFs) and contact-inhibited MEFs (ciMEFs).

References:

Agarwal, V., G. W. Bell, J.-W. Nam and D. P. Bartel. 2015. Predicting effective microRNA target sites in mammalian mRNAs. *elife* **4**: e05005.

Anders, S., P. T. Pyl and W. Huber. 2015. HTSeq—a Python framework to work with high-throughput sequencing data. *Bioinformatics* **31**: 166-169.

Ghini, F., C. Rubolino, M. Climent, I. Simeone, M. J. Marzi and F. Nicassio. 2018. Endogenous transcripts control miRNA levels and activity in mammalian cells by target-directed miRNA degradation. *Nat. Commun.* **9**: 3119.

Halbert, C., G. Demers and D. Galloway. 1991. The E7 gene of human papillomavirus type 16 is sufficient for immortalization of human epithelial cells. *J. Virol.* **65**: 473-478.

Kleaveland, B., C. Y. Shi, J. Stefano and D. P. Bartel. 2018. A network of noncoding regulatory RNAs acts in the mammalian brain. *Cell* **174**: 350-362. e317.

Martin, M. 2011. Cutadapt removes adapter sequences from high-throughput sequencing reads. *EMBnet J.* **17**: 10-12.

Ong, S.-E. and M. Mann. 2006. A practical recipe for stable isotope labeling by amino acids in cell culture (SILAC). *Nat. Protoc.* **1**: 2650.

Schwanhäusser, B., D. Busse, N. Li, G. Dittmar, J. Schuchhardt, J. Wolf, W. Chen and M. Selbach. 2011. Global quantification of mammalian gene expression control. *Nature* **473**: 337.

Wu, X. and D. P. Bartel. 2017. k pLogo: positional k-mer analysis reveals hidden specificity in biological sequences. *Nucleic Acids Res.* **45**: W534-W538.